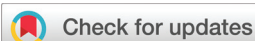


## RESEARCH ARTICLE

[View Article Online](#)  
[View Journal](#) | [View Issue](#)

 Cite this: *Inorg. Chem. Front.*, 2023,  
 10, 4763

# MOFs for long-term gas storage: exploiting kinetic trapping in ZIF-8 for on-demand and stimuli-controlled gas release†

 Karsten Heinz,<sup>a</sup> Sven M. J. Rogge,<sup>b</sup> Andreas Kalytta-Mewes,<sup>a</sup> Dirk Volkmer<sup>a</sup>  
 and Hana Bunzen<sup>a</sup>

In this study, we investigate the potential of metal–organic frameworks (MOFs) for long-term gas storage under ambient conditions. Specifically, we selected a MOF ZIF-8 (with a 0.34 nm large pore aperture), which exhibits a temperature- and pressure-regulated gating effect, and loaded it with sulphur hexafluoride (with a kinetic diameter of 0.55 nm). By optimising the loading conditions, we were able to achieve up to 33 wt% SF<sub>6</sub> loading into the pores of ZIF-8. Although MOFs featuring gating effects are known to adsorb gases larger than the pore openings, herein, by applying high pressure (and optionally elevated temperature), kinetic trapping of the gas guest was also achieved. When investigating the gas release under ambient conditions, three MOF samples of different crystal sizes (ca. 45 nm, 1.5 μm and 5 μm) were examined. Remarkably, for the largest crystals, more than 86% of the initially loaded gas remained trapped in the pores even after being exposed to air for 100 days under ambient conditions. Our findings indicate that the extremely slow release of SF<sub>6</sub> is due to the high activation energy for the guest diffusion through the narrow pore opening in ZIF-8, which was supported by both *ab initio*-based computational studies and experimental data including modulated thermogravimetric analysis. On the other hand, we also showed that the gas could be released on-demand by applying an elevated temperature or by exposing the MOF to an acidic environment, which opens possibilities for facile gas micro- and nano-dosing applications.

 Received 8th June 2023,  
 Accepted 26th June 2023

DOI: 10.1039/d3qi01007d

[rsc.li/frontiers-inorganic](https://rsc.li/frontiers-inorganic)

## Introduction

Metal–organic frameworks (MOFs) are porous coordination polymers.<sup>1–3</sup> They have attained great attention over the last more than two decades as they may be easily tailored<sup>4–8</sup> to the particular demands in various applications including gas storage and gas separation,<sup>9–16</sup> catalysis,<sup>17–22</sup> chemical sensing,<sup>23–26</sup> and biomedical applications.<sup>27–30</sup> Due to their crystalline nature, they have been regarded as rather rigid materials with stable and robust frameworks, and very often permanent porosity.<sup>31–33</sup> However, recent studies and the progress of our understanding of MOF structures have revealed

that flexibility appears to be more common than once thought.<sup>34–36</sup> MOFs exhibit a variety of flexible phenomena such as swelling, negative thermal expansion, gate opening, and breathing, especially when exposed to external stimulation.<sup>37–43</sup> For instance, many dynamic frameworks are temperature-responsive, allowing the structure of their pores as well as the apertures connecting them to deform, which inevitably influences guest admission and diffusion.<sup>44–47</sup> For instance, at the gate-opening temperature, apertures can open dynamically due to the thermal motion of the groups or ions delineating the aperture, and gas molecules can acquire sufficient kinetic energy to overcome the diffusion energy barrier and, thus, enter the pores. This phenomenon has been intensively studied in MOFs for gas separation.<sup>48,49</sup>

Among the different MOFs, ZIF-8 (zeolitic imidazolate framework-8; [Zn(MeIm)<sub>2</sub>]<sub>n</sub>, where MeIm is 2-methylimidazole)<sup>50</sup> has been the subject of a vast number of studies not only due to its thermal and water stability<sup>50</sup> and ease of synthesis,<sup>51,52</sup> but also because of its gating effect. ZIF-8 has a sodalite topology with large pores that are connected through narrow channels formed by a six-ligand-membered ring (Fig. 1a). The size of the pore aperture has been

<sup>a</sup>Chair of Solid State and Materials Chemistry, Institute of Physics, University of Augsburg, Universitaetsstrasse 1, 86159 Augsburg, Germany.

E-mail: hana.bunzen@physik.uni-augsburg.de

<sup>b</sup>Center for Molecular Modeling (CMM), Ghent University, Technologiepark-Zwijnaarde 46, B-9052 Ghent, Belgium

†Electronic supplementary information (ESI) available: Characterisation of ZIF-8; loading of SF<sub>6</sub>; release of SF<sub>6</sub> under ambient conditions; acid-triggered release; computational methods; computational free energy barriers for gas release. See DOI: <https://doi.org/10.1039/d3qi01007d>

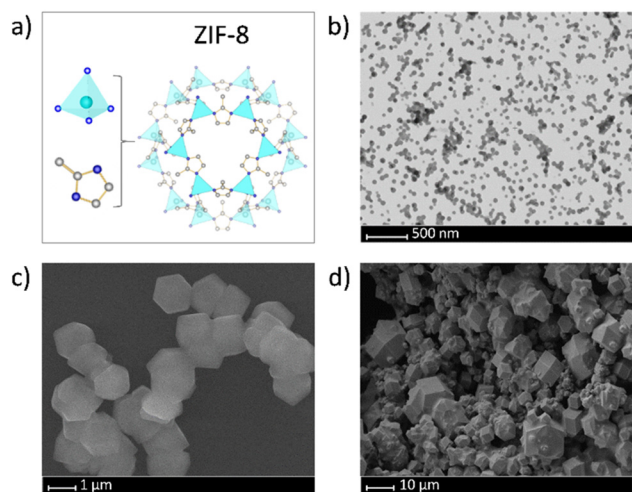


**Fig. 1** (a) Building blocks and the unit cell of ZIF-8, and electron micrographs of the ZIF-8 crystals studied in this work: (b) small – ZIF(s), (c) medium – ZIF(m), and (d) large – ZIF(l).

determined by single-crystal X-ray diffraction to be 0.34 nm.<sup>50</sup> However, results from gas permeation studies with different-sized molecules showed that ZIF-8 did not display a sharp molecular sieving cut-off at 0.34 nm, but that molecules with larger diameters than the pore aperture slowly permeated through.<sup>53,54</sup> This structural flexibility is called “gate-opening” or “swing-effect” and has been extensively studied by both theoretical and experimental methods.<sup>55–64</sup> For instance, Coudert *et al.* showed that ZIF-8 displays intraframework dynamics through the rotation of the 2-methylimidazolate linker.<sup>57</sup> The swinging of the linker can be caused by thermal fluctuations, as shown by *ab initio* molecular dynamics (MD) calculations,<sup>58</sup> or by the forces exerted by adsorbed molecules, as shown, for instance, by Fairen-Jimenez *et al.* using *in situ* powder X-ray diffraction.<sup>59</sup> The gate opening phenomenon can be identified in the gas adsorption isotherm as a sudden increase in the uptake that has been interpreted as a transition to a greater accessible pore volume in the material.<sup>59</sup> Moreover, the structural transition from the “closed” to the “open” pore state can be triggered not only by gas adsorption,<sup>59</sup> but also by mechanical pressure,<sup>65,66</sup> or even by an external electrical field.<sup>67</sup>

Although the gate opening phenomenon has been intensively studied in MOFs with regard to their potential applications in gas separation,<sup>48,49</sup> it has not been considered promising in gas adsorption, because physisorption is an exothermic phenomenon. Hence, low temperatures favour adsorption and promote host–guest interactions, while slightly higher temperatures are usually needed to induce the gating effect. Therefore, by achieving the gate opening temperature, the adsorption capacity and thus the overall loading tend to be reduced.<sup>68,69</sup> To effectively utilize the flexible opening for gas storage in MOFs, we propose to combine it with kinetic trapping of the guest. After inducing an external stimulus (*e.g.* pressure or/and temperature), the guest enters the pore

through the aperture, but after the stimulus is removed, it remains trapped inside the pore due to the drop in its kinetic energy. If a high gas pressure is used, a large amount of the guest can be trapped and stored inside the pores. This concept of kinetic trapping of gases in MOFs was introduced by us recently on an example of the MOF MFU-4 and xenon as a guest.<sup>70</sup> However, the guest release under ambient conditions was relatively fast and most of the gas was released within the first few days. In the current study, we selected ZIF-8 and SF<sub>6</sub> to demonstrate the possibility of utilizing kinetic trapping as an efficient tool for long-term gas storage in MOFs (in terms of both gas loading and release kinetics) under ambient conditions.

As a model guest, we selected sulphur hexafluoride (SF<sub>6</sub>) with a kinetic diameter of 0.55 nm.<sup>71</sup> SF<sub>6</sub> is used as a guest not only due to its molecular size (which is 1.6 times larger than the pore aperture of ZIF-8), but also because it is known as one of the most potent and persistent greenhouse gases.<sup>72,73</sup> Thus, the increasing industrial demand for SF<sub>6</sub> combined with severe environmental concerns calls for developing effective methods to ensure its safe storage and recovery. Furthermore, by employing ZIF-8 with its stimuli-induced gating phenomenon, on-demand gas release, controlled by external stimuli, can be expected, which can find applications in areas where precise gas dosing (especially micro- or even nano-dosing) is needed. For instance, in ophthalmology, during vitrectomy surgery, a small amount of SF<sub>6</sub> is often introduced into the eye in order to maintain the pressure required to allow the retina to remain in place and adequately heal.<sup>74,75</sup>

Last but not least, since it has been shown previously that crystal size can influence the adsorption process in framework materials,<sup>63,76</sup> we prepared ZIF-8 in three different crystal sizes and investigated gas desorption with regard to the crystal size in order to develop a system suitable for safe long-term gas storage.

## Results and discussion

### Material synthesis and characterisation

To study the effect of crystal size on the loading and release of SF<sub>6</sub> from ZIF-8, we prepared samples of ZIF-8 of three different crystal sizes, *ca.* 45 nm [sample ZIF-8(s); *s* = small], 1.5 μm [sample ZIF-8(m); *m* = medium] and 5 μm [sample ZIF-8(l); *l* = large] (Fig. 1, S4 and S5, ESI†), with the characteristic rhombic dodecahedron crystal morphology.<sup>77</sup> Synthesis and analytical data are given in the ESI (Fig. S1–S5, ESI†).

### SF<sub>6</sub> loading

To maximise the amount of SF<sub>6</sub> that could be stored in the different ZIF-8 samples, the loading temperature was optimized in 50 °C steps (Table S1, ESI†), while the pressure was kept constant at 20 bar (a higher pressure is not possible around room temperature, as SF<sub>6</sub> would liquify). The amount of the loaded gas was quantified by thermogravimetric analysis (TGA, Table S1, Fig. S7–S9, ESI†). Moreover, the samples were

also investigated by Fourier-transform infrared spectroscopy (FTIR, Fig. S14–S16, ESI†), which confirmed the presence of characteristic bands of SF<sub>6</sub>, and by X-ray powder diffraction (XRPD, Fig. S17–S19, ESI†), which did not reveal any changes in the framework cell parameters confirming the expected gas-induced gating phenomenon without a framework deformation.

With an increase of the crystal size, the loading temperature had to be increased to obtain comparably high loadings. As an alternative, the loading time could be prolonged too (Table S1, ESI†). The highest loading of 32.9 wt% (as determined by TGA, Fig. 2a and S7, ESI†) could be achieved for the sample ZIF-8(s) with the smallest crystal size already at 20 °C (*i.e.* at ambient temperature) after 18 h. A further increase of the temperature or loading time did not result in a higher loading, suggesting that the pores were filled. A loading of 32.9 wt% corresponds to 4.58 SF<sub>6</sub> molecules on average per pore, which is more than 76% of the calculated maximal possible occupancy of 6 molecules per pore. Moreover, the loading of 32.9 wt% corresponds to the volume of 75 mL of an ideal gas and a calculated SF<sub>6</sub> density of 0.496 g cm<sup>-3</sup> (see Table S1 details, ESI†), which is only 2.7 times lower than the density of the SF<sub>6</sub> liquid phase at

25 °C (1.329 g cm<sup>-3</sup>)<sup>78</sup> and 80 times higher than the density of SF<sub>6</sub> gas at 25 °C and 1 bar (6.164 × 10<sup>-3</sup> g cm<sup>-3</sup>).<sup>78</sup> In the case of the larger sample ZIF-8(m), the highest loading of 23.9 wt% was achieved at 150 °C and reduced compared to the sample ZIF-8(s), while for ZIF-8(l), the temperature had to be increased up to 200 °C to achieve a comparably lower loading of 18.5 wt% (Fig. 2a, Table S1, ESI†). Remarkably, in the cases of ZIF-8(s) and ZIF-8(m), SF<sub>6</sub> was gradually desorbed during the TGA measurement (well before reaching 350 °C), but in ZIF-8(l), we recorded an additional step at around 365 °C (Fig. 2b and S10, ESI†). This suggests that at this temperature the pore apertures were fully opened and the gas could freely diffuse out of the crystals. To exclude material decomposition at this temperature, TGA coupled with mass spectrometry was carried out (Fig. S11, ESI†). The measurement confirmed that the detected step change in the mass loss corresponded to the release of SF<sub>6</sub>. Moreover, FTIR and XRPD measurements (Fig. S12 and S13, ESI†) of samples after the TGA were carried out to show that the structure of ZIF-8 remained unchanged.

SF<sub>6</sub> molecules loaded into ZIF-8 pores were also detected by FTIR (Fig. 3 and S14–S16, ESI†). In the FTIR spectra, besides the bands corresponding to ZIF-8, additional bands were detected and assigned to the ν<sub>4</sub> (liquid: 610.8 cm<sup>-1</sup>; gas: 614.5 cm<sup>-1</sup>) and ν<sub>3</sub> (liquid: 914.9 cm<sup>-1</sup>; gas: 948.0 cm<sup>-1</sup>) vibration modes in SF<sub>6</sub>.<sup>79</sup> Remarkably, for the ν<sub>3</sub> vibration mode, two bands were detected, indicating that the state of some of the guest molecules is closer to the liquid phase while for others it is closer to the gas phase (Table S2, ESI†). This observation was investigated further during the gas release experiments (see the corresponding section and Fig. S26–S28, ESI†).

### Activation energy for gas molecules to move between pores

The activation energy needed for a molecule to pass from one pore to an adjacent pore was determined both experimentally and computationally. To determine the activation energy experimentally, modulated TGA (MTGA™ by TA Instruments), which uses an oscillation temperature program to obtain

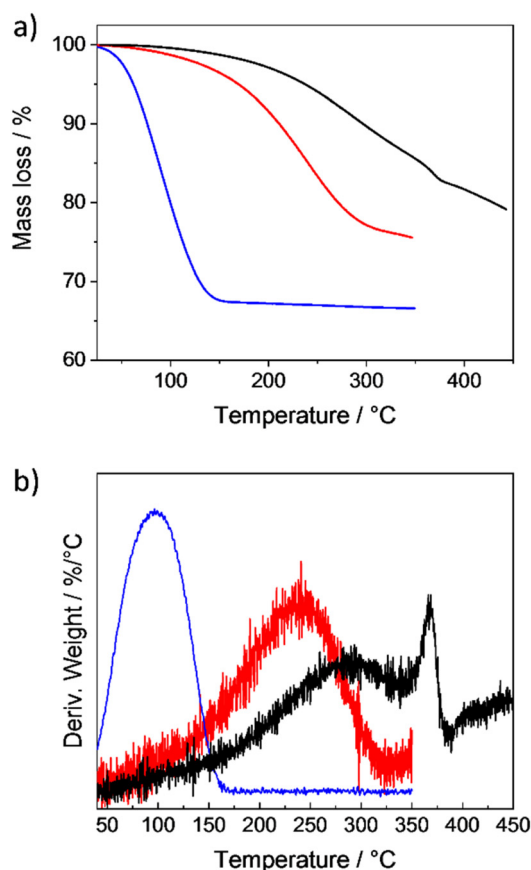


**Fig. 2** Thermogravimetric analysis of ZIF-8(s) (blue), ZIF-8(m) (red) and ZIF-8(l) (black) loaded with SF<sub>6</sub> under optimized conditions (Table S1, ESI†) shown as (a) mass loss vs. temperature and (b) deriv. weight (%/°C) vs. temperature.

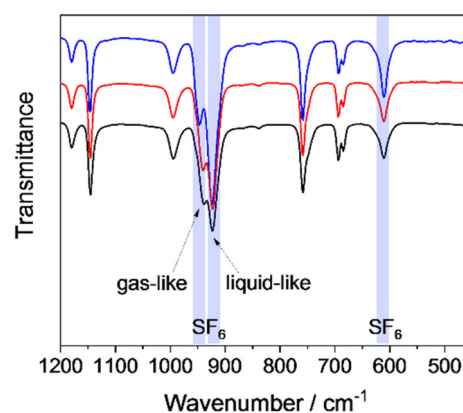


**Fig. 3** FTIR spectra of ZIF-8(s) (blue), ZIF-8(m) (red) and ZIF-8(l) (black) loaded with SF<sub>6</sub> under optimized conditions (Table S1, ESI†).

kinetic parameters during mass loss,<sup>80</sup> was employed. For all three samples, we measured an activation energy of *ca.* 80 kJ mol<sup>-1</sup> (Fig. S32, ESI†), which indicates, as one would expect, that there is no influence of the ZIF-8 particle size on the activation energy.

To understand the origin of the high activation barrier, we determined the free energy barrier for a SF<sub>6</sub> molecule to move from one ZIF-8 pore to an adjacent pore computationally. We adopted a procedure based on a series of umbrella sampling (US) simulations, similar to the one used in ref. 81 (see the ESI† for details). The guest location is defined by the collective variable (CV) shown in Fig. 4, which determines whether the SF<sub>6</sub> molecule is in the first pore (CV < 0 Å) or in the second, adjacent pore (CV > 0 Å). The six-membered ring (Fig. S35, ESI†) separating both pores is defined by CV = 0 Å and is expected to be responsible for the high activation barrier. This US protocol was necessary as SF<sub>6</sub> molecules were not observed to move from one pore to another spontaneously during a regular MD simulation at 300 K and 10 bar, a consequence of the large free energy barrier. Given the variable loading observed for the different pores, this analysis was repeated for different loadings of the first pore. Besides the SF<sub>6</sub> molecule that is constrained during the simulation, between zero and five additional SF<sub>6</sub> molecules were present in the first pore (CV < 0 Å). In contrast, the adjacent second pore (CV > 0 Å) contains no additional molecules. Fig. 4 shows the free energy profiles obtained in this fashion.

The first observation from this figure is that the free energy in the transition region around the aperture and the free energy in pore 2 are independent of the gas loading in pore 1, indicating that there is no appreciable interaction between SF<sub>6</sub> molecules residing in adjacent pores. This contrasts with earlier findings for water in ZIF-8, where hydrogen bonds formed between water molecules in adjacent pores were found

to be vital to facilitate the hopping of water from one pore to an adjacent pore.<sup>81</sup> As a result, the reverse free energy barrier (as seen from pore 2) amounts to *ca.* 110 kJ mol<sup>-1</sup>, irrespective of the loading in pore 1 (Fig. 4).

The second observation is that the forward free energy barrier does depend on the amount of SF<sub>6</sub> molecules in pore 1, varying between 100 and 130 kJ mol<sup>-1</sup>. The forward barrier reaches its maximum at intermediate loadings (Fig. S36, ESI†), given that the free energy of pore 1 is the lowest at that loading. This behaviour is explained in detail in section 6 of the ESI† and can be summarized as follows: when one additional SF<sub>6</sub> molecule is present in pore 1 (in orange, Fig. 4), dispersive guest-guest interactions stabilise the two molecules in pore 1, leading to a higher forward free energy barrier of about 132 kJ mol<sup>-1</sup>. At that point, any additional SF<sub>6</sub> molecule in pore 1 leads to steric hindrance that counteracts the attractive dispersive interactions. This is clearly seen when either two (in green) or three (in red) additional SF<sub>6</sub> molecules are present in pore 1 (Fig. 4 and S36, ESI†), as in that case the free energy in pore 1 is no longer flat but shows distinct minima. These minima correspond to favourable locations for the SF<sub>6</sub> molecules in which they optimise their mutual interactions and the interactions with the pore walls. Upon further increasing the number of SF<sub>6</sub> molecules in pore 1 (purple and brown profiles), steric hindrance starts to dominate, thereby increasing the free energy in pore 1 and lowering the forward free energy barrier to 100–110 kJ mol<sup>-1</sup> (Table S4†). All free energy barriers substantially exceed the already high free energy barriers encountered for water in ZIF-8 (16–25 kJ mol<sup>-1</sup>) and are in good agreement with the ones determined from modulated TGA.

### Release kinetics

Samples loaded under optimised loading conditions were exposed to air under ambient conditions and the amount of SF<sub>6</sub> in the pores was determined at regular time intervals up to 100 days by TGA (Fig. S20–S22, Table S3, ESI†). Moreover, FTIR and XRPD measurements were also carried out (Fig. S26–S31†). The experimental data confirmed that the kinetic trapping of SF<sub>6</sub> in the pores of ZIF-8 was successful. The large guest molecules could be loaded into ZIF-8 through the narrow pore apertures by applying an elevated pressure (and in some cases also temperature, Table S1, ESI†), but were not released immediately under ambient conditions in air.

The molecular exchange rate between porous crystals and their surroundings is known to be affected by both the permeation through the crystal surface (known as surface barrier resistance) and the diffusion through the intracrystalline pore network.<sup>82</sup> Thus, considering the different crystal sizes (Fig. 1 and S4, ESI†) of the three tested samples of ZIF-8, one would expect the impact of the crystal size parameter on the gas release to be significant. And indeed, as expected, the rate of release depended on the crystal size. The smaller the crystal size, the faster the overall release was (Fig. 5 and S23, ESI†). However, even in the case of ZIF-8(s), it took more than 21 days to achieve complete gas release (with only less than

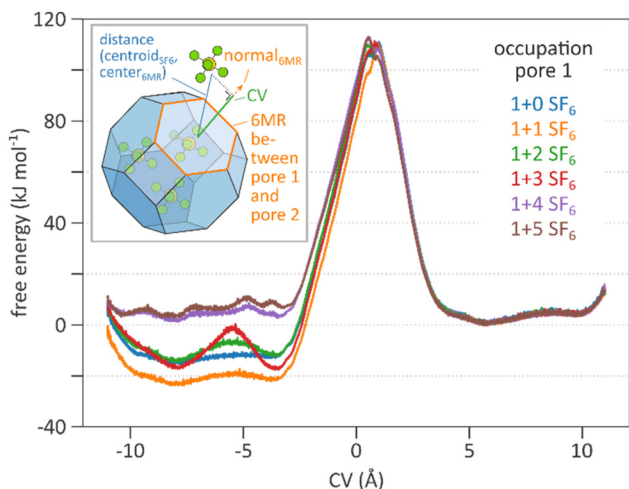


**Fig. 4** 300 K free energy profiles for the hopping of one SF<sub>6</sub> molecule from pore 1 (CV < 0 Å) to the adjacent pore 2 (CV > 0 Å). In these simulations, between zero and five additional SF<sub>6</sub> molecules are present in pore 1, while no additional molecules are present in pore 2.

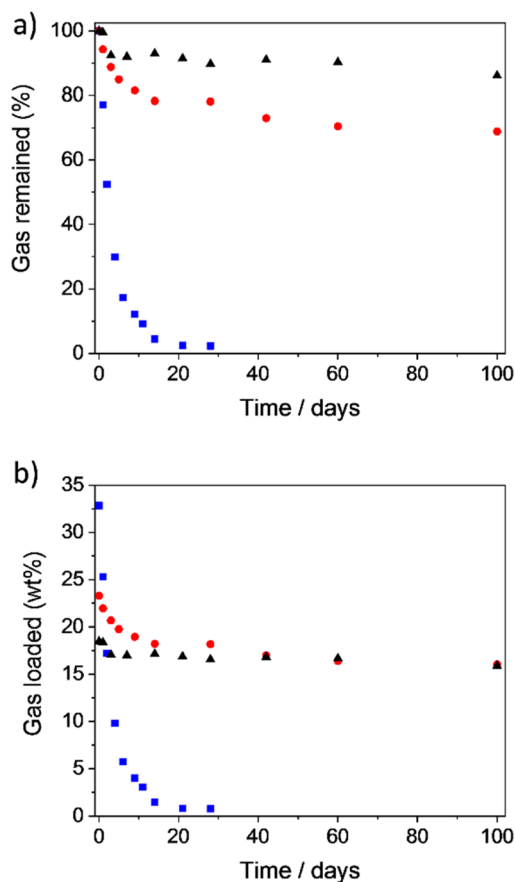


**Fig. 5** Gas release under ambient conditions from ZIF-8(s) (blue), ZIF-8(m) (red) and ZIF-8(l) (black) loaded with SF<sub>6</sub> under optimized conditions (Table S1, ESI†) expressed (a) as % of the remained gas and (b) as wt% of loaded gas in the pores; determined by TGA (Fig. S20–S22, ESI†).

1 wt% of SF<sub>6</sub> left inside the pores), although it took only about 2 days to achieve 50% release of the originally loaded amount of SF<sub>6</sub> from these smallest crystals. In contrast, by increasing the crystals to the micro-sized regime, the release was slowed down significantly. In the cases of ZIF-8(m) and ZIF-8(l), even after 100 days of exposing both samples to air at ambient temperature, more than 68% and 86%, respectively, of the originally loaded amount of SF<sub>6</sub> remained inside the pores. This confirms the high activation barriers derived both experimentally and computationally above. It also means that the pores of ZIF-8 themselves served as “nanotanks” for long-term gas storage without the need for an additional vessel.

To further quantify the molecular transport in the ZIF-8 crystals, we assumed the SF<sub>6</sub> particles to be spherical (which is a rather accepted simplification<sup>83,84</sup>). The gas diffusivity was then determined from the release curves (Fig. S25, ESI†), by fitting the intra-crystalline (Fick) diffusion model<sup>82</sup> on the experimental data (see section 3 in the ESI† for details). Assuming an isothermal release behaviour and that the diffusivity is loading-independent, the diffusion time constants were determined to be  $0.12 \times 10^{-21} \text{ m}^2 \text{ s}^{-1}$  for ZIF-8(s),  $1.58 \times 10^{-21} \text{ m}^2 \text{ s}^{-1}$  for ZIF-8(m) and  $4.93 \times 10^{-21} \text{ m}^2 \text{ s}^{-1}$  for ZIF-8(l)

(Table S4, ESI†). The difference in these constants indicates that the release is not only driven by the intracrystalline diffusion, but also that the surface resistance governs the overall diffusion rate. These findings are in agreement with the results reported by Tanaka and Denayer *et al.*, who observed that *n*-butanol uptake in small crystallites of ZIF-8 (0.06–2.1 μm) was limited by surface barriers, while the diffusion rate of larger crystallites (88 μm) was governed by intra-crystalline diffusion.<sup>85</sup> It is noteworthy that the found values are also in agreement with the computationally determined infinite dilution self-diffusion coefficient of SF<sub>6</sub> in ZIF-8 reported by Sholl *et al.* recently:  $1.73 \times 10^{-22} \text{ m}^2 \text{ s}^{-1}$  at 0 °C and  $3.73 \times 10^{-21} \text{ m}^2 \text{ s}^{-1}$  at 35 °C.<sup>56</sup>

Last but not least, the guest release could also be determined by FTIR spectroscopy (Fig. S26–S28, ESI†). With the gradual release of SF<sub>6</sub>, the intensity of the band corresponding to the  $\nu_3$  vibration mode of the liquid-like guest (around 925 cm<sup>-1</sup>) decreased, while the intensity of the band corresponding to the gas-like guest (around 947 cm<sup>-1</sup>) was first unchanged and only after the band of the liquid-like phase disappeared, it was reduced gradually too (Fig. S26–S28, ESI†).

### Gas release on demand

To trigger the gas release on demand, either an elevated temperature (Fig. S10, ESI†) or an acidic environment (Fig. S33, ESI†) can be applied. The acid-triggered release studies showed that by adding an acid (herein 2 M HCl as an example), ZIF-8 readily decomposed, and the gas could be released immediately (Fig. S33, ESI†). A video capturing the whole experiment is available as an ESI.† Such an approach can find applications in areas where a precise dosing of gases in small amounts is needed (such as the application of SF<sub>6</sub> gas in ophthalmology<sup>74,75</sup>), because due to the solid nature of the samples, it is very easy to handle such materials and to weigh their amounts precisely.

## Conclusions

Herein, we reported on an efficient strategy of long-term gas storage and on-demand gas release in MOFs by utilizing MOFs with a prominent flexible pore opening combined with kinetic trapping. In this approach, after inducing an external stimulus (herein pressure and temperature), the gaseous guest enters the MOF pores through the aperture, and after the stimulus is removed, it remains trapped inside due to the drop in its kinetic energy. In such an approach, large quantities of gas can be introduced and stored in the MOF pores as we showed here by storing SF<sub>6</sub> in the pores of ZIF-8. We demonstrated that such systems could be used for long-term storage of gases at ambient temperature and pressure without the need for a high-pressure container, or in fact any container. The capture of SF<sub>6</sub> inside the pores is a result of the high activation barriers of *ca.* 80 kJ mol<sup>-1</sup> of the SF<sub>6</sub> diffusion through the pores. Furthermore, we also showed that the gas can be released on-demand by applying an elevated temperature or acid treat-

ment. Finally, due to their solid nature, such materials are easy to handle and thus, they have great potential in applications requiring precise gas dosing, especially in micro- and nano-dosing applications.

## Experimental

### Materials and experimental methods

All chemicals were of reagent grade and used as received from commercial suppliers. Fourier transform infrared (FTIR) spectra were recorded in the range of 400–4000  $\text{cm}^{-1}$  on a Bruker Equinox 55 FT-IR spectrometer equipped with an ATR unit. X-ray powder diffraction (XRPD) patterns were collected using a Seifert XRD 3003 TT powder diffractometer with a Meteor1D detector using  $\text{Cu K}\alpha_1$  radiation ( $\lambda = 1.54187 \text{ \AA}$ ). The thermogravimetric analysis (TGA) was performed with a TGA Q500 analyser in the temperature range from 25 °C up to 700 °C under a nitrogen atmosphere at a heating rate of 10 K  $\text{min}^{-1}$ . To determine the activation energy, modulated TGA was carried out under a helium atmosphere at a heating rate of 2 K  $\text{min}^{-1}$ , with an amplitude of  $\pm 5 \text{ }^\circ\text{C}$  and a period of 200 s. Scanning electron microscopy (SEM) and scanning transmission electron microscopy (STEM) micrographs were recorded with a Crossbeam 550 microscope (Zeiss) and optical microscopy photographs were taken with an Olympus IX70 microscope equipped with a camera.

### Synthesis of ZIF-8

**ZIF-8(small, s).** The material synthesis was adapted from a previously reported procedure.<sup>86</sup>  $\text{Zn}(\text{NO}_3)_2 \cdot 6\text{H}_2\text{O}$  (734 mg, 2.47 mmol) and 2-methylimidazole (811 mg, 9.87 mmol) were each dissolved in 50 mL of methanol, and then both solutions were poured together and briefly mixed. The reaction mixture was left undisturbed for 1 h. After that, the precipitate was collected by centrifugation, washed three times with methanol and dried in an oven at 60 °C overnight. The product was obtained as a white powder (176 mg, yield calculated on the basis of  $\text{Zn}(\text{II})$ : 31%).

**ZIF-8(medium, m).** The material synthesis was adapted from a previously reported procedure.<sup>86</sup>  $\text{Zn}(\text{NO}_3)_2 \cdot 6\text{H}_2\text{O}$  (734 mg, 2.47 mmol) was dissolved in 50 mL of methanol. In another 50 mL of methanol, 2-methylimidazole (811 mg, 9.87 mmol) and sodium formate (671.5 mg, 9.87 mmol) were dissolved. Both solutions were poured together and briefly mixed. The reaction mixture was left undisturbed for 48 h. After that, the precipitate was collected by centrifugation, washed three times with methanol and dried in an oven at 60 °C overnight. The product was obtained as a white powder (51 mg, yield calculated on the basis of  $\text{Zn}(\text{II})$ : 9%).

**ZIF-8(large, l).** The material synthesis was adapted from a previously reported procedure.<sup>87</sup>  $\text{ZnCl}_2$  (60.6 mg, 0.22 mmol), 2-methylimidazole (73.0 mg, 0.44 mmol) and sodium formate (60.6 mg, 0.44 mmol) were dissolved in 6 mL of methanol. The reaction mixture was placed in a heating tube, closed tightly and heated at 130 °C for 4 h. After cooling down, the precipi-

tate was collected by filtration, washed three times with methanol and dried in an oven at 60 °C overnight. The product was obtained as a white powder (75 mg, yield calculated on the basis of  $\text{Zn}(\text{II})$ : 74%).

### Gas loading

For each experiment, 20–100 mg of ZIF-8 were placed into a steel vessel constructed from metal tubing attached to a manometer (Fig. S6†). The vessel was filled with  $\text{SF}_6$  gas and kept at the desired pressure and temperature for the desired period of time. Upon cooling down, the gas pressure was released and the sample (*ca.* 5–10 mg) was immediately analysed with TGA, FTIR and XRPD methods.

Precautionary statement: these experiments involve  $\text{SF}_6$  gas under high pressure. Measures and suitable equipment for working with gas under pressure need to be in place to ensure safety and to minimize and prevent any risks.

### Gas release

The gas loaded samples were kept in a container exposed to air. After a certain period of time a small amount (*ca.* 5–10 mg) was taken and analysed by TGA, FTIR and XRPD methods.

### Computational studies

The procedure to arrive at the computational free energy profiles in Fig. 4 consists of four steps. First, a force field for  $\text{SF}_6$  was derived based on density functional theory (DFT) input data following the QuickFF protocol,<sup>88,89</sup> and combined with an earlier derived DFT-based force field for ZIF-8.<sup>81</sup> Second, a CV was defined to describe the transition of a  $\text{SF}_6$  molecule between two adjacent pores in ZIF-8. Third, regular MD simulations were performed to obtain realistic initial structures for the US simulations and to rule out any spontaneous transitions. Fourth, US simulations were performed to finally extract the free energy profiles. Representative input scripts are available at <https://github.com/SvenRogge/supporting-info>; further details about these procedures are given in section 5 of the ESI.†

## Author contributions

KH carried out the material synthesis and characterisation as well as the gas loading and release studies. SMJR carried out the computational studies. AKM carried out the MTGA measurements. DV contributed to the conceptualization of the work. HB conceptualized the work and carried out electron microscopy studies. All authors contributed to the article writing.

## Conflicts of interest

There are no conflicts to declare.

## Acknowledgements

HB acknowledges the financial support from the German Research Foundation (SPP 1928, COORNETS). SMJR acknowledges support from the Fund for Scientific Research Flanders (FWO) through a postdoctoral fellowship (grant no. 12T3522N). The computational resources and services used in this work were provided by the VSC (Flemish Supercomputer Center), funded by the Research Foundation – Flanders (FWO) and the Flemish Government – department EWI.

## References

- H. Furukawa, K. E. Cordova, M. O’Keeffe and O. M. Yaghi, The Chemistry and Applications of Metal-Organic Frameworks, *Science*, 2013, **341**, 1230444.
- H.-C. Zhou, J. R. Long and O. M. Yaghi, Introduction to Metal-Organic Frameworks, *Chem. Rev.*, 2012, **112**, 673–674.
- Y. Bai, Y. Dou, L.-H. Xie, W. Rutledge, J.-R. Li and H.-C. Zhou, Zr-based metal-organic frameworks: design, synthesis, structure, and applications, *Chem. Soc. Rev.*, 2016, **45**, 2327–2367.
- Z.-J. Lin, J. Lü, M. Hong and R. Cao, Metal-organic frameworks based on flexible ligands (FL-MOFs): structures and applications, *Chem. Soc. Rev.*, 2014, **43**, 5867–5895.
- A. Kirchon, L. Feng, H. F. Drake, E. A. Joseph and H.-C. Zhou, From fundamentals to applications: a toolbox for robust and multifunctional MOF materials, *Chem. Soc. Rev.*, 2018, **47**, 8611–8638.
- A. Schoedel, M. Li, D. Li, M. O’Keeffe and O. M. Yaghi, Structures of Metal-Organic Frameworks with Rod Secondary Building Units, *Chem. Rev.*, 2016, **116**, 12466–12535.
- Z. Chen, H. Jiang, M. Li, M. O’Keeffe and M. Eddaoudi, Reticular Chemistry 3.2: Typical Minimal Edge-Transitive Derived and Related Nets for the Design and Synthesis of Metal-Organic Frameworks, *Chem. Rev.*, 2020, **120**, 8039–8065.
- Q.-G. Zhai, X. Bu, X. Zhao, D.-S. Li and P. Feng, Pore Space Partition in Metal-Organic Frameworks, *Acc. Chem. Res.*, 2017, **50**, 407–417.
- M. P. Suh, H. J. Park, T. K. Prasad and D.-W. Lim, Hydrogen Storage in Metal-Organic Frameworks, *Chem. Rev.*, 2012, **112**, 782–835.
- M. Ding, R. W. Flaig, H.-L. Jiang and O. M. Yaghi, Carbon capture and conversion using metal-organic frameworks and MOF-based materials, *Chem. Soc. Rev.*, 2019, **48**, 2783–2828.
- W. Fan, X. Zhang, Z. Kang, X. Liu and D. Sun, Isoreticular chemistry within metal-organic frameworks for gas storage and separation, *Coord. Chem. Rev.*, 2021, **443**, 213968.
- J.-R. Li, Y. Ma, M. C. McCarthy, J. Sculle, J. Yu, H.-K. Jeong, P. B. Balbuena and H.-C. Zhou, Carbon dioxide capture-related gas adsorption and separation in metal-organic frameworks, *Coord. Chem. Rev.*, 2011, **255**, 1791–1823.
- J.-R. Li, R. J. Kuppler and H.-C. Zhou, Selective gas adsorption and separation in metal-organic frameworks, *Chem. Soc. Rev.*, 2009, **38**, 1477–1504.
- B. Seoane, J. Coronas, I. Gascon, M. E. Benavides, O. Karvan, J. Caro, F. Kapteijn and J. Gascon, Metal-organic framework based mixed matrix membranes: a solution for highly efficient CO<sub>2</sub> capture?, *Chem. Soc. Rev.*, 2015, **44**, 2421–2454.
- M. S. Denny, J. C. Moreton, L. Benz and S. M. Cohen, Metal-organic frameworks for membrane-based separations, *Nat. Rev. Mater.*, 2016, **1**, 16078.
- R.-B. Lin, S. Xiang, H. Xing, W. Zhou and B. Chen, Exploration of porous metal-organic frameworks for gas separation and purification, *Coord. Chem. Rev.*, 2019, **378**, 87–103.
- A. Dhakshinamoorthy, Z. Li and H. Garcia, Catalysis and photocatalysis by metal organic frameworks, *Chem. Soc. Rev.*, 2018, **47**, 8134–8172.
- L. Jiao, Y. Wang, H.-L. Jiang and Q. Xu, Metal-Organic Frameworks as Platforms for Catalytic Applications, *Adv. Mater.*, 2018, **30**, 1703663.
- Q. Yang, Q. Xu and H.-L. Jiang, Metal-organic frameworks meet metal nanoparticles: synergistic effect for enhanced catalysis, *Chem. Soc. Rev.*, 2017, **46**, 4774–4808.
- T. Zhang and W. Lin, Metal-organic frameworks for artificial photosynthesis and photocatalysis, *Chem. Soc. Rev.*, 2014, **43**, 5982–5993.
- L. Zhu, X.-Q. Liu, H.-L. Jiang and L.-B. Sun, Metal-Organic Frameworks for Heterogeneous Basic Catalysis, *Chem. Rev.*, 2017, **117**, 8129–8176.
- Y.-Z. Chen, R. Zhang, L. Jiao and H.-L. Jiang, Metal-organic framework-derived porous materials for catalysis, *Coord. Chem. Rev.*, 2018, **362**, 1–23.
- J. F. Olorunyomi, S. T. Geh, R. A. Caruso and C. M. Doherty, Metal-organic frameworks for chemical sensing devices, *Mater. Horiz.*, 2021, **8**, 2387–2419.
- L. E. Kreno, K. Leong, O. K. Farha, M. Allendorf, R. P. Van Duyne and J. T. Hupp, Metal-Organic Framework Materials as Chemical Sensors, *Chem. Rev.*, 2012, **112**, 1105–1125.
- Y. Shen, A. Tissot and C. Serre, Recent progress on MOF-based optical sensors for VOC sensing, *Chem. Sci.*, 2022, **13**, 13978–14007.
- Y. Cui, J. Zhang, H. He and G. Qian, Photonic functional metal-organic frameworks, *Chem. Soc. Rev.*, 2018, **47**, 5740–5785.
- P. Horcajada, R. Gref, T. Baati, P. K. Allan, G. Maurin, P. Couvreur, G. Férey, R. E. Morris and C. Serre, Metal-Organic Frameworks in Biomedicine, *Chem. Rev.*, 2012, **112**, 1232–1268.
- X. Ma, M. Lepoitevin and C. Serre, Metal-organic frameworks towards bio-medical applications, *Mater. Chem. Front.*, 2021, **5**, 5573–5594.
- E. Linnane, S. Haddad, F. Melle, Z. Mei and D. Fairen-Jimenez, The uptake of metal-organic frameworks: a journey into the cell, *Chem. Soc. Rev.*, 2022, **51**, 6065–6086.

- 30 H. Bunzen and D. Jirak, Recent Advances in Metal–Organic Frameworks for Applications in Magnetic Resonance Imaging, *ACS Appl. Mater. Interfaces*, 2022, **14**, 50445–50462.
- 31 S. Yuan, L. Feng, K. Wang, J. Pang, M. Bosch, C. Lollar, Y. Sun, J. Qin, X. Yang, P. Zhang, Q. Wang, L. Zou, Y. Zhang, L. Zhang, Y. Fang, J. Li and H.-C. Zhou, Stable Metal–Organic Frameworks: Design, Synthesis, and Applications, *Adv. Mater.*, 2018, **30**, 1704303.
- 32 I. M. Hönicke, I. Senkowska, V. Bor, I. A. Baburin, N. Bönisch, S. Raschke, J. D. Evans and S. Kaskel, Balancing Mechanical Stability and Ultrahigh Porosity in Crystalline Framework Materials, *Angew. Chem., Int. Ed.*, 2018, **57**, 13780–13783.
- 33 A. J. Howarth, Y. Liu, P. Li, Z. Li, T. C. Wang, J. T. Hupp and O. K. Farha, Chemical, thermal and mechanical stabilities of metal–organic frameworks, *Nat. Rev. Mater.*, 2016, **1**, 15018.
- 34 D. N. Dybtsev, H. Chun and K. Kim, Rigid and Flexible: A Highly Porous Metal–Organic Framework with Unusual Guest-Dependent Dynamic Behavior, *Angew. Chem., Int. Ed.*, 2004, **43**, 5033–5036.
- 35 S. Horike, S. Shimomura and S. Kitagawa, Soft porous crystals, *Nat. Chem.*, 2009, **1**, 695–704.
- 36 T. D. Bennett, A. H. Fuchs, A. K. Cheetham and F.-X. Coudert, Flexibility and disorder in metal–organic frameworks, *Dalton Trans.*, 2016, **45**, 4058–4059.
- 37 A. Schneemann, V. Bon, I. Schwedler, I. Senkowska, S. Kaskel and R. A. Fischer, Flexible metal–organic frameworks, *Chem. Soc. Rev.*, 2014, **43**, 6062–6096.
- 38 F.-X. Coudert, Responsive Metal–Organic Frameworks and Framework Materials: Under Pressure, Taking the Heat, in the Spotlight, with Friends, *Chem. Mater.*, 2015, **27**, 1905–1916.
- 39 T. D. Bennett, A. K. Cheetham, A. H. Fuchs and F.-X. Coudert, Interplay between defects, disorder and flexibility in metal–organic frameworks, *Nat. Chem.*, 2017, **9**, 11–16.
- 40 L. Vanduyfhuys, S. M. J. Rogge, J. Wieme, S. Vandenbrande, G. Maurin, M. Waroquier and V. Van Speybroeck, Thermodynamic insight into stimuli-responsive behaviour of soft porous crystals, *Nat. Commun.*, 2018, **9**, 204.
- 41 J. H. Lee, S. Jeoung, Y. G. Chung and H. R. Moon, Elucidation of flexible metal–organic frameworks: Research progresses and recent developments, *Coord. Chem. Rev.*, 2019, **389**, 161–188.
- 42 J. D. Evans, V. Bon, I. Senkowska, H.-C. Lee and S. Kaskel, Four-dimensional metal–organic frameworks, *Nat. Commun.*, 2020, **11**, 2690.
- 43 S. Krause, N. Hosono and S. Kitagawa, Chemistry of Soft Porous Crystals: Structural Dynamics and Gas Adsorption Properties, *Angew. Chem., Int. Ed.*, 2020, **59**, 15325–15341.
- 44 F.-X. Coudert, A. Boutin, A. H. Fuchs and A. V. Neimark, Adsorption Deformation and Structural Transitions in Metal–Organic Frameworks: From the Unit Cell to the Crystal, *J. Phys. Chem. Lett.*, 2013, **4**, 3198–3205.
- 45 C. Gu, N. Hosono, J.-J. Zheng, Y. Sato, S. Kusaka, S. Sakaki and S. Kitagawa, Design and control of gas diffusion process in a nanoporous soft crystal, *Science*, 2019, **363**, 387–391.
- 46 A. Gonzalez-Nelson, F.-X. Coudert and M. A. van der Veen, Rotational Dynamics of Linkers in Metal–Organic Frameworks, *Nanomaterials*, 2019, **9**, 330.
- 47 A. Sharma, N. Dwarkanath and S. Balasubramanian, Thermally activated dynamic gating underlies higher gas adsorption at higher temperatures in metal–organic frameworks, *J. Mater. Chem. A*, 2021, **9**, 27398–27407.
- 48 K. Chen, S. H. Mousavi, R. Singh, R. Q. Snurr, G. Li and P. A. Webley, Gating effect for gas adsorption in microporous materials—mechanisms and applications, *Chem. Soc. Rev.*, 2022, **51**, 1139–1166.
- 49 S. Hiraide, Y. Sakanaka, H. Kajiro, S. Kawaguchi, M. T. Miyahara and H. Tanaka, High-throughput gas separation by flexible metal–organic frameworks with fast gating and thermal management capabilities, *Nat. Commun.*, 2020, **11**, 3867.
- 50 K. S. Park, Z. Ni, A. P. Côté, J. Y. Choi, R. Huang, F. J. Uribe-Romo, H. K. Chae, M. O’Keeffe and O. M. Yaghi, Exceptional chemical and thermal stability of zeolitic imidazolate frameworks, *Proc. Natl. Acad. Sci. U. S. A.*, 2006, **103**, 10186–10191.
- 51 Y.-R. Lee, M.-S. Jang, H.-Y. Cho, H.-J. Kwon, S. Kim and W.-S. Ahn, ZIF-8: A comparison of synthesis methods, *Chem. Eng. J.*, 2015, **271**, 276–280.
- 52 Q. Wang, Y. Sun, S. Li, P. Zhang and Q. Yao, Synthesis and modification of ZIF-8 and its application in drug delivery and tumor therapy, *RSC Adv.*, 2020, **10**, 37600–37620.
- 53 C. Zhang, R. Lively, K. Zhang, J. R. Johnson, O. Karvan and W. J. Koros, Unexpected Molecular Sieving Properties of Zeolitic Imidazolate Framework-8, *J. Phys. Chem. Lett.*, 2012, **3**, 2130–2134.
- 54 K. Eum, K. C. Jayachandrababu, F. Rashidi, K. Zhan, J. Leisen, S. Graham, R. P. Lively, R. R. Chance, D. S. Sholl, C. W. Jones and S. Nair, Highly Tunable Molecular Sieving and Adsorption Properties of Mixed-Linker Zeolitic Imidazolate Frameworks, *J. Am. Chem. Soc.*, 2015, **137**, 4191–4197.
- 55 J. G. Vitillo and L. Gagliardi, Modeling Metal Influence on the Gate Opening in ZIF-8 Materials, *Chem. Mater.*, 2021, **33**, 4465–4473.
- 56 R. J. Verploegh, S. Nair and D. S. Sholl, Temperature and Loading-Dependent Diffusion of Light Hydrocarbons in ZIF-8 as Predicted Through Fully Flexible Molecular Simulations, *J. Am. Chem. Soc.*, 2015, **137**, 15760–15771.
- 57 F.-X. Coudert, Molecular Mechanism of Swing Effect in Zeolitic Imidazolate Framework ZIF-8: Continuous Deformation upon Adsorption, *ChemPhysChem*, 2017, **18**, 2732–2738.
- 58 T. Watanabe and D. S. Sholl, Accelerating Applications of Metal–Organic Frameworks for Gas Adsorption and Separation by Computational Screening of Materials, *Langmuir*, 2012, **28**, 14114–14128.

- 59 D. Fairen-Jimenez, S. A. Moggach, M. T. Wharmby, P. A. Wright, S. Parsons and T. Düren, Opening the Gate: Framework Flexibility in ZIF-8 Explored by Experiments and Simulations, *J. Am. Chem. Soc.*, 2011, **133**, 8900–8902.
- 60 S. Ohsaki, S. Watanabe, H. Tanaka and M. T. Miyahara, Free Energy Analysis for Adsorption-Induced Structural Transition of Colloidal Zeolitic Imidazolate Framework-8 Particles, *J. Phys. Chem. C*, 2017, **121**, 20366–20374.
- 61 R. Boada, J. Chaboy, S. Hayama, L. L. Keenan, A. A. Freeman, M. Amboage and S. Diaz-Moreno, Unraveling the Molecular Details of the “Gate Opening” Phenomenon in ZIF-8 with X-ray Absorption Spectroscopy, *J. Phys. Chem. C*, 2022, **126**, 5935–5943.
- 62 T. Ueda, T. Yamatani and M. Okumura, Dynamic Gate Opening of ZIF-8 for Bulky Molecule Adsorption as Studied by Vapor Adsorption Measurements and Computational Approach, *J. Phys. Chem. C*, 2019, **123**, 27542–27553.
- 63 T. Tian, M. T. Wharmby, J. B. Parra, C. O. Ania and D. Fairen-Jimenez, Role of crystal size on swing-effect and adsorption induced structure transition of ZIF-8, *Dalton Trans.*, 2016, **45**, 6893–6900.
- 64 M. E. Casco, Y. Q. Cheng, L. L. Daemen, D. Fairen-Jimenez, E. V. Ramos-Fernández, A. J. Ramirez-Cuesta and J. Silvestre-Albero, Gate-opening effect in ZIF-8: the first experimental proof using inelastic neutron scattering, *Chem. Commun.*, 2016, **52**, 3639–3642.
- 65 S. A. Moggach, T. D. Bennett and A. K. Cheetham, The Effect of Pressure on ZIF-8: Increasing Pore Size with Pressure and the Formation of a High-Pressure Phase at 1.47 GPa, *Angew. Chem., Int. Ed.*, 2009, **48**, 7087–7089.
- 66 C. L. Hobday, C. H. Woodall, M. J. Lennox, M. Frost, K. Kamenev, T. Düren, C. A. Morrison and S. A. Moggach, Understanding the adsorption process in ZIF-8 using high pressure crystallography and computational modelling, *Nat. Commun.*, 2018, **9**, 1429.
- 67 A. Knebel, B. Geppert, K. Volgmann, D. I. Kolokolov, A. G. Stepanov, J. Twiefel, P. Heitjans, D. Volkmer and J. Caro, Defibrillation of soft porous metal-organic frameworks with electric fields, *Science*, 2017, **358**, 347–351.
- 68 J. Shang, G. Li, Q. Gu, R. Singh, P. Xiao, J. Z. Liu and P. A. Webley, Temperature controlled invertible selectivity for adsorption of N<sub>2</sub> and CH<sub>4</sub> by molecular trapdoor chabazites, *Chem. Commun.*, 2014, **50**, 4544–4546.
- 69 D. Kim, J. Park, Y. S. Kim and M. S. Lah, Temperature dependent CO<sub>2</sub> behavior in microporous 1-D channels of a metal-organic framework with multiple interaction sites, *Sci. Rep.*, 2017, **7**, 41447.
- 70 H. Bunzen, F. Kolbe, A. Kalytta-Mewes, G. Sastre, E. Brunner and D. Volkmer, Achieving Large Volumetric Gas Storage Capacity in Metal–Organic Frameworks by Kinetic Trapping: A Case Study of Xenon Loading in MFU-4l, *J. Am. Chem. Soc.*, 2018, **140**, 10191–10197.
- 71 T. Hasell, M. Miklitz, A. Stephenson, M. A. Little, S. Y. Chong, R. Clowes, L. Chen, D. Holden, G. A. Tribello, K. E. Jelfs and A. I. Cooper, Porous Organic Cages for Sulfur Hexafluoride Separation, *J. Am. Chem. Soc.*, 2016, **138**, 1653–1659.
- 72 S. Xiao, X. Zhang, J. Tang and S. Liu, A review on SF<sub>6</sub> substitute gases and research status of CF<sub>3</sub>I gases, *Energy Rep.*, 2018, **4**, 486–496.
- 73 X. Fang, X. Hu, G. Janssens-Maenhout, J. Wu, J. Han, S. Su, J. Zhang and J. Hu, Sulfur hexafluoride (SF<sub>6</sub>) emission estimates for China: an inventory for 1990–2010 and a projection to 2020, *Environ. Sci. Technol.*, 2013, **47**, 3848–3855.
- 74 A. Kontos, J. Tee, A. Stuart, Z. Shalchi and T. H. Williamson, Duration of intraocular gases following vitreoretinal surgery, *Graefe’s Arch. Clin. Exp. Ophthalmol.*, 2017, **255**, 231–236.
- 75 W. I. Sabates, G. W. Abrams, D. E. Swanson and E. W. Norton, The use of intraocular gases. The results of sulfur hexafluoride gas in retinal detachment surgery, *Ophthalmology*, 1981, **88**, 447–454.
- 76 C. L. Hobday, S. Krause, S. M. J. Rogge, J. D. Evans and H. Bunzen, Perspectives on the Influence of Crystal Size and Morphology on the Properties of Porous Framework Materials, *Front. Chem.*, 2021, **9**, 772059.
- 77 J. Troyano, A. Carné-Sánchez, C. Avci, I. Imaz and D. Maspoch, Colloidal metal–organic framework particles: the pioneering case of ZIF-8, *Chem. Soc. Rev.*, 2019, **48**, 5534–5546.
- 78 [https://www.chemeurope.com/en/encyclopedia/Sulfur\\_hexafluoride.html](https://www.chemeurope.com/en/encyclopedia/Sulfur_hexafluoride.html) (accessed on 30.05.23).
- 79 C. Chapados and G. Birnbaum, Infrared absorption of SF<sub>6</sub> from 32 to 3000 cm<sup>-1</sup> in the gaseous and liquid states, *J. Mol. Spectrosc.*, 1988, **132**, 323–351.
- 80 R. L. Blaine and B. K. Hahn, Comparison of Activation Energies Obtained from Modulated and Conventional Non-modulated TG, *J. Therm. Anal. Calorim.*, 1997, **54**, 695–704.
- 81 Y. Sun, S. M. J. Rogge, A. Lamaire, S. Vandenbrande, J. Wieme, C. R. Siviour, V. Van Speybroeck and J.-C. Tan, High-rate nanofluidic energy absorption in porous zeolitic frameworks, *Nat. Mater.*, 2021, **20**, 1015–1023.
- 82 J. Kärger, Transport Phenomena in Nanoporous Materials, *ChemPhysChem*, 2015, **16**, 24–51.
- 83 C. Y. Lee, Y. S. Bae, N. C. Jeong, O. K. Farha, A. A. Sarjeant, C. L. Stern, P. Nickias, R. Q. Snurr, J. T. Hupp and S. T. Nguyen, Kinetic Separation of Propene and Propane in Metal–Organic Frameworks: Controlling Diffusion Rates in Plate-Shaped Crystals via Tuning of Pore Apertures and Crystallite Aspect Ratios, *J. Am. Chem. Soc.*, 2011, **133**, 5228–5231.
- 84 H. Lee, W. S. Chi, M. J. Lee, K. Zhang, F. Edhaim, K. M. Rodriguez, S. J. A. DeWitt and Z. P. Smith, Network-Nanostructured ZIF-8 to Enable Percolation for Enhanced Gas Transport, *Adv. Funct. Mater.*, 2022, **32**, 2207775.
- 85 S. Tanaka, K. Fujita, Y. Miyake, M. Miyamoto, Y. Hasegawa, T. Makino, S. Van der Perre, J. Cousin Saint Remi, T. Van Assche, G. V. Baron and J. F. M. Denayer, Adsorption and Diffusion Phenomena in Crystal Size Engineered ZIF-8 MOF, *J. Phys. Chem. C*, 2015, **119**, 28430–28439.

- 86 J. Cravillon, R. Nayuk, S. Springer, A. Feldhoff, K. Huber and M. Wiebcke, Controlling Zeolitic Imidazolate Framework Nano- and Microcrystal Formation: Insight into Crystal Growth by Time-Resolved In Situ Static Light Scattering, *Chem. Mater.*, 2011, **23**, 2130–2141.
- 87 J. Cravillon, C. A. Schröder, H. Bux, A. Rothkirch, J. Caro and M. Wiebcke, Formate modulated solvothermal synthesis of ZIF-8 investigated using time-resolved in situ X-ray diffraction and scanning electron microscopy, *CrystEngComm*, 2012, **14**, 492–498.
- 88 L. Vanduyfhuys, S. Vandenbrande, T. Verstraelen, R. Schmid, M. Waroquier and V. Van Speybroeck, QuickFF: A program for a quick and easy derivation of force fields for metal-organic frameworks from ab initio input, *J. Comput. Chem.*, 2015, **36**, 1015–1027.
- 89 L. Vanduyfhuys, S. Vandenbrande, J. Wieme, M. Waroquier, T. Verstraelen and V. Van Speybroeck, Extension of the QuickFF force field protocol for an improved accuracy of structural, vibrational, mechanical and thermal properties of metal-organic frameworks, *J. Comput. Chem.*, 2018, **39**, 999–1011.